Boron Phosphide van der Waals *p-n* Junction via Molecular Adsorption

Y. Mogulkoc,[1] M. Modarresi,[2] A. Mogulkoc,[3,*] and B. Alkan[1]

[1]*Department of Engineering Physics, Faculty of Engineering, Ankara University, 06100 Tandogan, Ankara, Turkey*

[2]*Department of Physics, Ferdowsi University of Mashhad, Mashhad, Iran*

[3]*Department of Physics, Faculty of Sciences, Ankara University, 06100 Tandogan, Ankara, Turkey*

We propose a *p-n* junction diode based on the adsorption of tetrathiafulvalene (TTF) and tetracyanoquinodimethane (TCNQ) molecules on a monolayer of boron phosphide (MBP). We use density functional theory and a simple tight-binding model to investigate atomic configuration, electronic properties, and transport characteristics of the TCNQ/MBP/TTF structure. The *p-n* mechanism is achieved by the full coverage of MBP with TCNQ and TTF molecules, which are coupled by weak van der Waals forces. The adsorption of each individual molecule on MBP provides localized electronic states close to the valence and conduction bands; this is characteristic of *p*- and *n*-type semiconductors. To understand the charge-carrier dynamics, we also examine the evaluation of energy bands, together with localized states, local potential, charge redistribution, and charge transfer under the influence of an external electric field. Our results show that the adsorption of both molecules on the surfaces of MBP results in the behavior of a *p-n* junction with a rectifying current through the junction in the proposed van der Waals device. Moreover, the optical response to electromagnetic radiation is also analyzed through density functional theory by considering the independent-particle approximation. We show that, with a remarkable absorption band in the infrared region, TCNQ/MBP/TTF is a potential candidate as a component of next-generation optoelectronic devices.

I. INTRODUCTION

With the synthesis of graphene, two-dimensional (2D) layered materials, such as phosphorene [1–3], group IV monolayers [4–9], and transition-metal dichalcogenides [10], have become the focus of scientific research, owing to silicon technology having reached the limit with respect to the shrinkage of devices. The electronic structure of 2D layered phases, unlike their bulk counterparts, exhibit different characteristics, such as direct-indirect band-gap transitions, and metallic, semiconductor, and insulating behavior, depending on the number of layers and stacking order [11–14]. Their flexible and wide range of functional features make them potential building blocks for next-generation nanoelectronic devices. In practice, the technologically applicable capacity of materials is precisely dependent on tuning and the value of the electronic energy band gap. Some of the methods followed to achieve this aim are the construction of heterostructures from these 2D sheets, doping, adsorption of organic molecules, application of an external electric field, and structural strain. Many recent experimental and theoretical studies have

reported that van der Waals heterostructures, consisting of combining different 2D phases formed vertically and laterally, show very different electronic and optical properties than those of their individual components [15–23]. The external electric field modifies the electronic bands. For instance, van der Waals heterostructure studies on MoS_2/stanene [18], $GaSe/MoS_2$ [19], and GeC/WS_2 [20] show that the external electric field changes the magnitude of the band gap and yields direct or indirect energy band-gap transitions. Another highly preferred technique to modulate the electronic and optical properties of the substrate is molecular adsorption. Tetracyanoquinodimethane (TCNQ) and tetrathiafulvalene (TTF) molecules are the focus of research in the field of molecular electronics, owing to their low ionization energies and high affinity properties, which allow easy electron transfer from TTF to TCNQ. In other words, owing to the overlap of energetic molecular orbitals, this TCNQ-TTF structure becomes a metallic phase, and therefore, an electric current, consisting of electrons and holes, flows perpendicular to the planes of the molecules [24,25]. In addition, to the properties of *n*- and *p*-type semiconductors, TCNQ-TTF, with effective charge-carrier injection, can be used as an alternative electrode to inorganic electrodes,

*mogulkoc@science.ankara.edu.tr

such as Au and Ag, in optoelectronics [26,27]. Accordingly, Lu and co-workers [28] investigated the adsorption of electron-accepting tetracyanoethylene (TCNE) on graphene, using first-principles density functional theory (DFT) and reported that p-type graphene could be achieved through charge transfer, and that the coverage of organic molecules was an effective option to control the electronic features of graphene [29]. On the other hand, the adsorption of three organic molecules with different characteristics on phosphorene was studied by Yu *et al.* [30] through DFT. The infrared absorption of molybdenum disulfide (MoS_2) monolayer is enhanced by molecular charge transfer to TCNQ [31]. The construction of p- and n-type semiconductors can be achieved by doping p- and n-type elements [32–35], stacking of heterostructures [36–38], and molecular adsorption [39–42]. Recently, Gao *et al.* [42] reported the functionalization of an arsenene monolayer with TCNQ and TTF as donor and acceptor molecules, respectively, and studied the electronic current through a p-n junction. Moreover, Çakır *et al.* [43] explained the realization of a two-dimensional p-n junction through doping of a monolayer of boron phosphide (MBP).

Here, we propose a nanoscale p-n junction based on the adsorption of organic molecules on MBP. We examine the impact of molecular adsorption on the electronic and optical properties of MBP by considering first-principle calculations. First, we consider half-coverage of the MBP layer with TCNQ and TTF, then we extend the idea to construct a p-n junction mechanism by considering full coverage of the MBP layer with TCNQ and TTF, which are held by weak van der Waals interactions. We show that the surface adsorption of TCNQ and TTF on MBP can lead to p- and n-type doped semiconductors. Moreover, the formation of the p-n junction is suggested through simultaneous adsorption of TCNQ and TTF molecules on both surfaces of MBP. We analyze the electronic properties of the structures by considering energy bands, charge transfer, and local potential in the absence and presence of an external electric field. The DFT electronic states are used to parameterize a simple tight-binding model for the calculation of current-voltage characteristics by using the Green function and Landauer-Buttiker formalism. Finally, we examine the optical spectrum of doped structures through the calculation of the imaginary part of the dielectric function within the framework of linear response theory.

II. METHODS

All first-principles calculations are performed by using the Vienna *ab initio* Simulation Package (VASP) [44,45]. The generalized gradient approximation (GGA) with the Perdew-Burke-Ernzerhof (PBE) functional is used to approximate the exchange-correlation potential [46]. The energy cutoff for a plane-wave basis is set

to 500 eV. For each configuration, the atomic positions and lattice constants are optimized by using the quasi-Newton method. For atomic relaxation, the final maximum Hellmann-Feynman force on each atom is less than 0.01 eV/Å. Brillouin zone integration is performed by using the gamma-centered Monkhorst-Pack algorithm [47] of $8 \times 8 \times 1$ k points for a $4 \times 4 \times 1$ supercell containing 16 B and 16 P atoms of MBP. A 30 Å vacuum is set along the perpendicular direction to the MBP to avoid interactions with the nearest unit cell. The convergence criterion for total-energy minimization is set to 10^{-7} eV between two sequential steps. To take into account the van der Waals (vdW) interactions between weakly bound 2D layers, we use the DFT-D2 method [48]. In VASP, the electric field is considered by adding an artificial dipole sheet in the middle of the vacuum in the unit cell [49]. The hybrid Heyd-Scuseria-Ernzerhof (HSE) [50,51] functional provides a better estimation of the electronic energy band gap, with respect to available experimental measurements and GW approximation, as a higher level model [52,53]. Owing to the high computational cost for the large supercell, HSE calculations are limited to the electronic band structure and optical spectrum of TCNQ/MBP/TTF (see the Supplemental Material [54] for DFT HSE bands).

The electron partition between different layers is investigated by using Bader charge analysis, as implemented in a code developed by Henkelman *et al.* [55–57]. By considering the total energies of MBP and molecules, the adsorption energy (E_{ad}) per unit cell of the system is calculated as,

$$E_{ad} = E_{MBP} + E_{TCNQ} + E_{TTF} - E_{TCNQ/MBP/TTF},$$

where E_{MBP}, E_{TCNQ}, and E_{TTF} correspond to the total energy of isolated MBP, TCNQ, and TTF layers, respectively. $E_{TCNQ/MBP/TTF}$ is the total energy of the TCNQ/MBP/TTF system. On the other hand, the charge density difference of each system is calculated by

$$\Delta\rho = \rho_{TCNQ/MBP/TTF} - \rho_{MBP} - \rho_{TCNQ} - \rho_{TTF},$$

where $\rho_{TCNQ/MBP/TTF}$, ρ_{MBP}, ρ_{TCNQ}, and ρ_{TTF} are the charge densities of the TCNQ/MBP/TTF system and isolated MBP, TCNQ, and TTF layers, respectively.

Moreover, we calculate the current-voltage characteristics of TCNQ/MBP/TTF by using a simplified tight-binding (TB) model. The electronic current is calculated through the Green function formalism [58,59] by connecting the p-n junction between source and drain electrodes. The effect of two electrodes is modeled with the self-energy operator ($\Sigma_{L,R}$), which can be obtained by using the surface Green function and molecule-electrode coupling strength [58]. Here, for simplicity, the left and right electrodes are described in the wide-band approximation, which estimates the self-energy operator of

electrodes with an energy-independent pure imaginary matrix [60]. The retarded Green function of the *p-n* junction between the electrodes can be written as $G^r(E) = [E - H - \Sigma_L - \Sigma_R]^{-1}$, where H is the TB model Hamiltonian. The current-voltage characteristics are calculated by using the Landauer-Buttiker formalism, $I(V) = (2e/h) \int dE \, \text{trace} \left[\Gamma_L G^r(E) \Gamma_R G^a(E) \right] (f_L - f_R)$, where $\Gamma_{L,R} = -2 \, \text{Im}(\Sigma_{L,R})$, $G^a = (G^r)^\dagger$ is the advanced Green function and $f_{L,R}$ is the Fermi function for the left and right electrodes.

Furthermore, we examine the optical properties of MBP after the adsorption of TCNQ and TTF through DFT by using the GGA PBE functional without a local field effect. The linear response of a system due to external electromagnetic radiation is described by the complex dielectric function $\varepsilon(\omega) = \varepsilon_1(\omega) + i\varepsilon_2(\omega)$. The dispersion of the imaginary part of the complex dielectric function, $\varepsilon_2(\omega)$, is derived from the momentum matrix elements between the occupied and unoccupied wave functions, as follows [61],

$$\varepsilon_2^{(\alpha\beta)} = \frac{4\pi^2 e^2}{\Omega} \lim_{q \to 0} \frac{1}{q^2} \sum_{c,v,\mathbf{k}} 2\omega_{\mathbf{k}} \delta \left(\epsilon_{c,\mathbf{k}} - \epsilon_{v,\mathbf{k}} - \omega \right)$$

$$\times \left\langle u_{c,\mathbf{k}+\mathbf{e}_\alpha q} | u_{v,\mathbf{k}} \right\rangle \left\langle u_{c,\mathbf{k}+\mathbf{e}_\beta q} | u_{v,\mathbf{k}} \right\rangle^*,$$

where c and v correspond to the conduction and valence band states, respectively, and $u_{c\mathbf{k}}$ is the cell periodic part of the orbitals at the *k* point $\mathbf{k}$.

III. RESULTS

A. Electronic properties in the absence of electric field

We first present the atomic configuration and electronic bands of MBP doped with TCNQ and TTF molecules. The atomic bond length of B–P is 1.86 Å, which is compatible with earlier studies [15,16,43,62], and does not change after the adsorption of TCNQ and TTF molecules. Different atomic positions are examined for each molecule on the MBP to find the minimum-energy configuration of TCNQ/MBP and TTF/MBP, as shown in Fig. 1, which is the most favorable adsorption configuration. Other more energetic and less favorable possible positions for the adsorption of TCNQ and TTF are presented in the Supplemental Material [54]. At the lowest energy configuration of TCNQ, the adsorption height ($d_{\text{TCNQ/MBP}}$) is 3.43 Å above MBP. For the TTF molecule, the adsorption height ($d_{\text{MBP/TTF}}$) is 3.18 Å above MBP. The center of the hexagon in TCNQ is above a B atom and TTF is slightly shifted with respect to hexagons in MBP. The definition of the adsorption energy (E_{ad}) is given in Sec. II as the energy difference between that of MBP/TCNQ(TTF) and isolated MBP and TCNQ(TTF). The adsorption energies (E_{ad}) for TCNQ/MBP and MBP/TTF interfaces are 113 meV and 100 meV, respectively. The calculated values are compatible with the adsorption energy of the same molecules on a monolayer of hexagonal boron nitride [63], which has a similar structure to that of MBP as a member of III–V binary compounds. In the adsorption of both
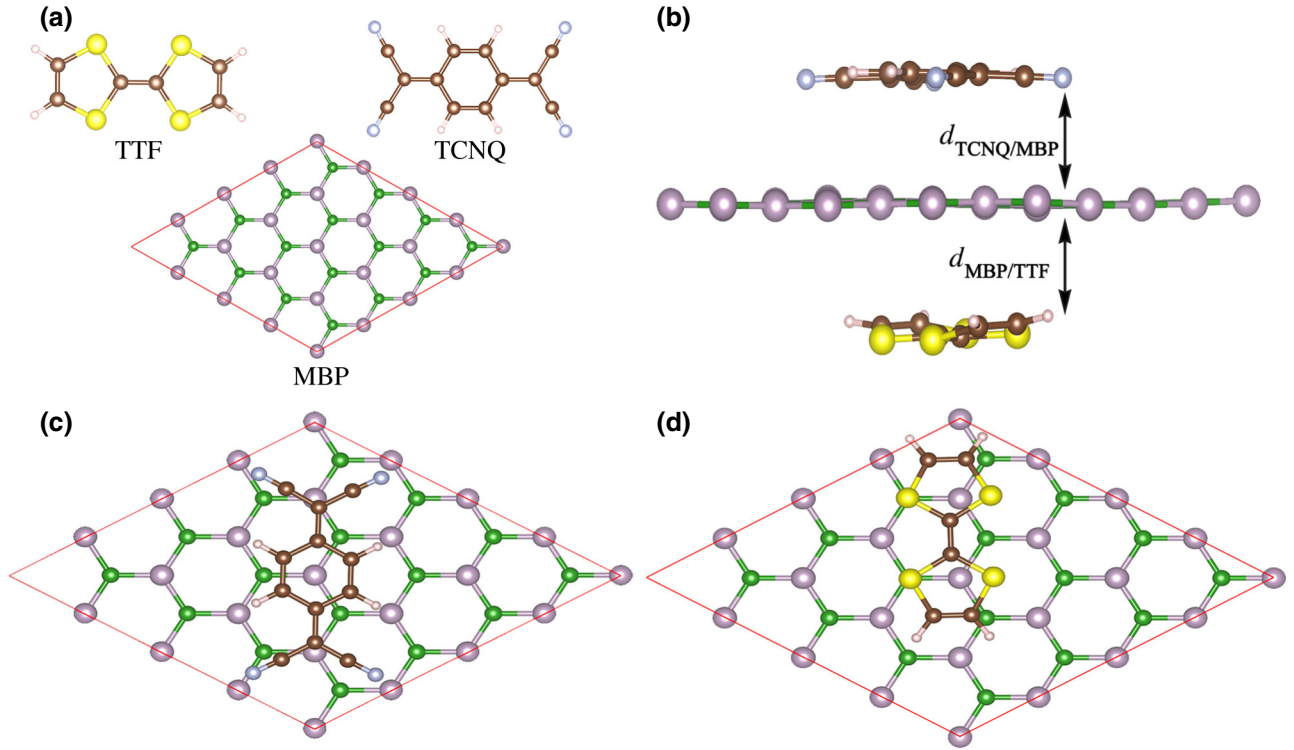

FIG. 1.   Lowest energy configurations of (a) TCNQ, TTF, and MBP; (b) TCNQ/MBP/TTF; (c) TCNQ/MBP; and (d) MBP/TTF.

molecules, the adsorption energy of the TCNQ/MBP/TTF system becomes 82 meV lower than that of interfacial adsorption of each molecule. The atomic structure of MBP is almost unchanged after adsorption of molecules; this can be attributed to low adsorption energies due to weak vdW interlayer interactions of molecules. The energy difference between the lowest energy configuration and other considered atomic configurations is in the range of 2–197 meV (2–80 meV) for TCNQ (TTF) molecules (see the Supplemental Material [54] for details). A possible experimental mechanism for full coverage can be considered as the liquid exfoliation of MBP and functionalization with TCNQ and TTF molecules in the solution phase. A similar method is used for the functionalization of other 2D monolayers [64–67].

As shown in Fig. 2(a), MBP is a direct semiconductor with an energy band gap of 0.90 eV between the valence band maximum (VBM) and the conduction band minimum (CBM) at the K point of 1BZ, which is compatible with early results [15,16,43]. Figures 2(b) and 2(c) represent the projected electronic bands for TCNQ and TTF layers on MBP. The red and blue (green) lines correspond to the contributions of MBP and TCNQ (TTF) layers, respectively, to the band structure. One can easily recognize that the electronic bands consist of MBP electronic bands and a localized state from each molecule close to the Fermi level (E_F). Here, E_F is set to be zero in Figs. 2 and 4. Even the shapes of the electronic bands of MBP remain almost unchanged by molecular adsorption; the presence of TCNQ (TTF) shifts the conduction
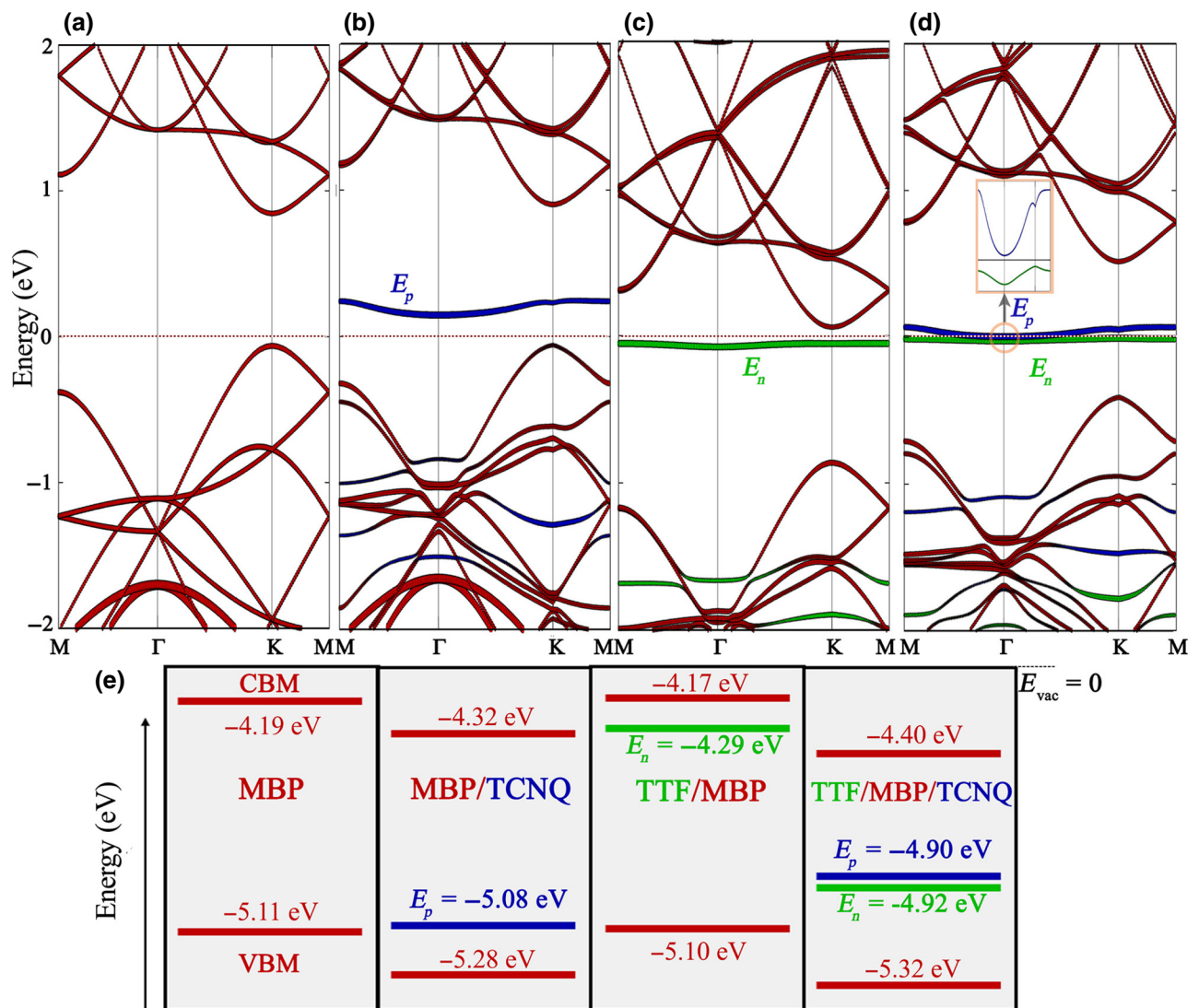

FIG. 2. Projected electronic band structures for (a) 4×4 MBP, (b) MBP/TCNQ, (c) MBP/TTF, and (d) TCNQ/MBP/TTF. Projected bands on MBP, TCNQ, and TTF are shown in red, blue, and green, respectively. The Fermi level is set to zero and is shown by a dotted line. (e) Schematic representation of the band alignment of the structures.

and valance band states of MBP far away from the Fermi level, which is clear in Figs. 2(b) and 2(c). The adsorption of TCNQ provides an empty localized band in the energy band gap close to valence bands, which is a feature of *p*-doped semiconductors [Fig. 2(b)]. On the other hand, the adsorption of TTF molecules shows characteristics of a *n*-doped semiconductor, with a filled shallow localized state near the conduction band, as shown in Fig. 2(c). The molecular localized energy states are presented as $E_{p(n)} = -5.08(-4.29)$ eV, with respect to the vacuum energy level [see Fig. 2(e)]. Here, $E_{p,n}$ is the energy of localized states belonging to *p*- and *n*-type doping, according to the Fermi energy in the band spectrum. The partial bands in Figs. 2(b)–2(d) show that the localized bands are purely related to TCNQ and TTF molecules. The VBM of bulk bands at the TCNQ/MBP interface has contributions from both the MBP layer and TCNQ molecules. For TTF/MBP, both the VBM and CBM of bulk bands at the *K* point result from MBP. The electronic band gap in the *p*- and *n*-type semiconductors are sharply reduced to 0.21 eV between ΓK points and 0.11 eV at the *K* point from the original MBP band gap, respectively. In the TCNQ/MBP/TTF system, the energy band spectrum includes flat bands of *p*- and *n*-type states at $E_p = -4.90$ eV and $E_n = -4.92$ eV, respectively, with respect to vacuum energy. The electronic bands of MBP (red color) show a wide band gap of 0.93 eV in Fig. 2(d). There is also one localized empty band from TCNQ and one filled shallow band from TTF inside the band gap. Upon the adsorption of two molecules, the CBM (VBM) shifts to lower (higher) energy with respect

to pristine MBP and it yields a tiny electronic band gap of 20 meV between two localized states from TCNQ and TTF at the DFT PBE level [as shown in the inset of Fig. 2(d)]. The electronic band spectrum of TCNQ/MBP/TTF is also obtained by using DFT HSE06, which has the same trend as that with PBE, and yields a band gap of around approximately 0.68 eV (see the Supplemental Material [54] for details). For the four atomic configurations, we draw the band alignment by considering vacuum level as a reference energy in Fig. 2(e). The energy levels are comparable due to the unique energy reference. The energy level related to MBP is almost unchanged by the adsorption of TTF, while both the VBM and CBM of MBP are shifted by the adsorption of TCNQ. Interestingly, the relative positions of molecular levels change in TCNQ/MBP/TTF with respect to the adsorption of individual molecules. For example, the energy difference between the VBM of MBP and TCNQ is 0.2 eV for TCNQ/MBP, which increases to 0.58 eV for TCNQ/MBP/TTF.

In the Bader charge analysis of interfaces, charge transfer from MBP to TCNQ is 0.30 |*e*|, while TTF (MBP) loses (gains) 0.09 |*e*| at the TCNQ/MBP and MBP/TTF interfaces, respectively. The quantity of charge transfer is increased by the full coverage of MBP with TTF and TCNQ. While TCNQ gains 0.42 |*e*|, TTF loses 0.27 |*e*| for TCNQ/MBP/TTF. As a result, MBP also gains a net charge of +0.15 |*e*|, which is a desired feature, such that MBP behaves like a spacer between molecules instead of a charge accumulator; thus charge transfer substantially occurs between two molecules. Charge transfer between
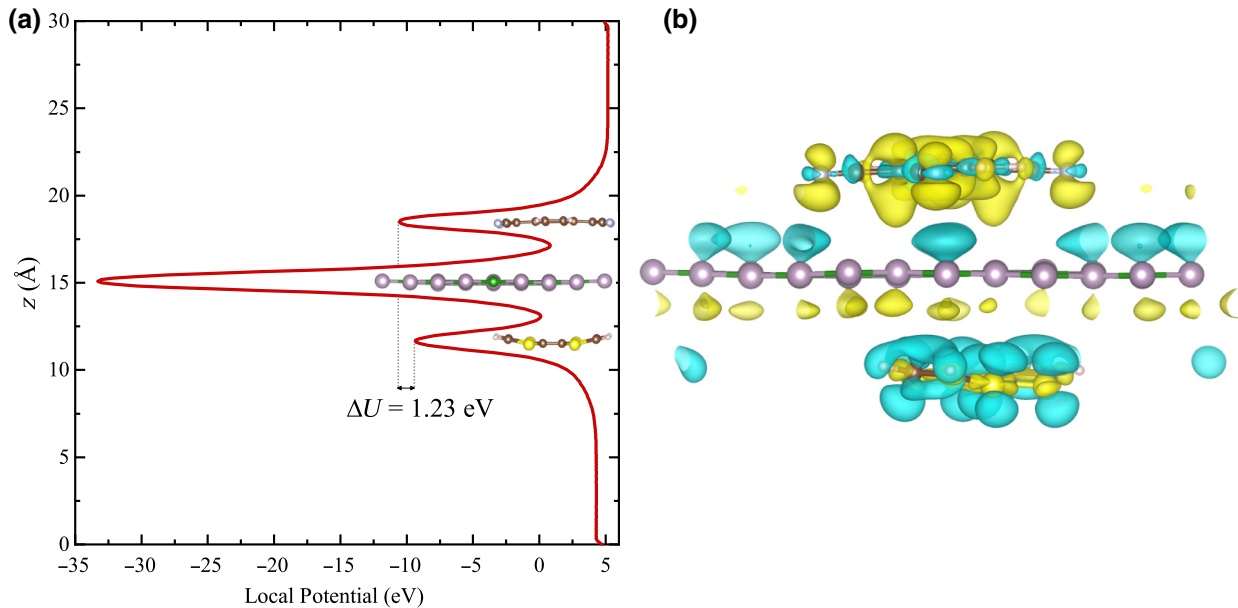

FIG. 3. (a) Plane-averaged electrostatic potential along the normal direction of a monolayer for the TCNQ/MBP/TTF structure. (b) Charge-density difference of the TCNQ/MBP/TTF system. Yellow and blue colors represent charge accumulation and depletion, respectively. The isosurface value is set to be 0.0006 eÅ^{-3}.

layers is also calculated based on the DDEC6 method [68,69]. Due to similar charge-transfer regimes, they are not presented here (see the Supplemental Material [54] for details). In semiconductor technology, p- and n-type semiconductors are attached side by side to form a p-n junction, which works as an electronic rectifying diode. Here, our idea is that the TCNQ and TTF molecules on both sides of MBP act as a p-n junction.

For a deeper insight into the adsorption process, the plane-averaged electrostatic potential and charge-density distribution after the adsorption of TCNQ and TTF on MBP are presented in Fig. 3. Moreover, the photoelectric threshold (work function) of the structures can be calculated by using the electrostatic potential [Fig. 3(a)], which is an important feature for the design of electronic and photovoltaic devices [29,70]. The work function is defined as $\Phi_w = E^{\mathrm{vac}} - E_F$, where E^{vac} is the vacuum electrostatic potential of the structure. Here, E_F is set to zero in Fig. 3. The work function of MBP is $\Phi_w = 4.66$ eV [16]. It is calculated that the adsorption of TCNQ molecules increases the work function to $\Phi_w = 5.23$ eV, while the adsorption of TTF decreases it to $\Phi_w = 4.19$ eV. In the full coverage of both molecules, the work function of

TCNQ/MBP/TTF is $\Phi_w = 4.72$ eV ($\Phi_w = 4.91$ eV) for the TCNQ/MBP (MBP/TTF) side of the interface. Similar effects of acceptor and donor molecules on the work function of a 2D material are reported in Refs. [71] and [72]. The relative magnitude of the work functions of adsorbed structures can be associated with charge transfer between molecules and MBP, which occurs from a low work function structure to a high work function structure [73,74]. The work function difference ($\Delta\Phi_w$) between TCNQ/MBP (MBP/TTF) and pure MBP is 0.57 eV (-0.47 eV) for the interfaces. It is clear from the work function scheme that charge transfer occurs from MBP (TTF) to TCNQ (MBP) for the TCNQ/MBP (MBP/TTF) interface, which is compatible with the results of Bader charge analysis. Moreover, charge transfer from TTF to TCNQ is also supported by the work function ($\Phi_w^{\mathrm{MBP/TTF}} > \Phi_w^{\mathrm{TCNQ/MBP}}$) for full coverage of MBP. The charge density difference in Fig. 3(b) shows a charge accumulation (depletion) region on TCNQ (TTF), which confirms the p- and n-type semiconductor characteristics, as discussed for the electronic band structure in Fig. 2. Charge redistribution occurs mainly on molecules, rather than at the interfacial region, while TCNQ (TTF) gains (loses) charge. It is also
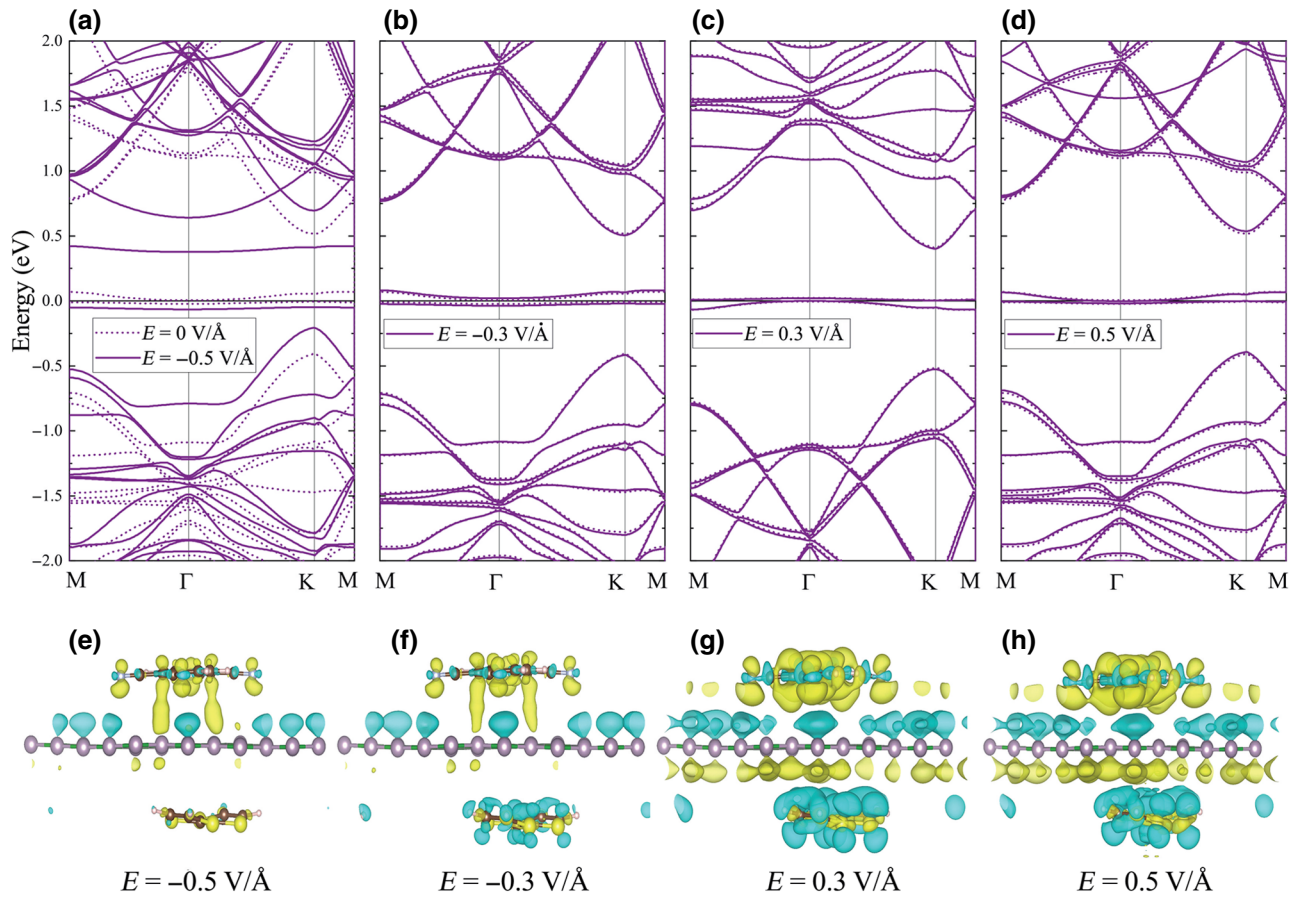

FIG. 4.   (a)–(d) Electronic band structure and (e)–(h) charge-density difference of TCNQ/MBP/TTF at an external electric field. The isosurface value is set to 0.0006 e$\mathrm{\mathring{A}}^{-3}$.
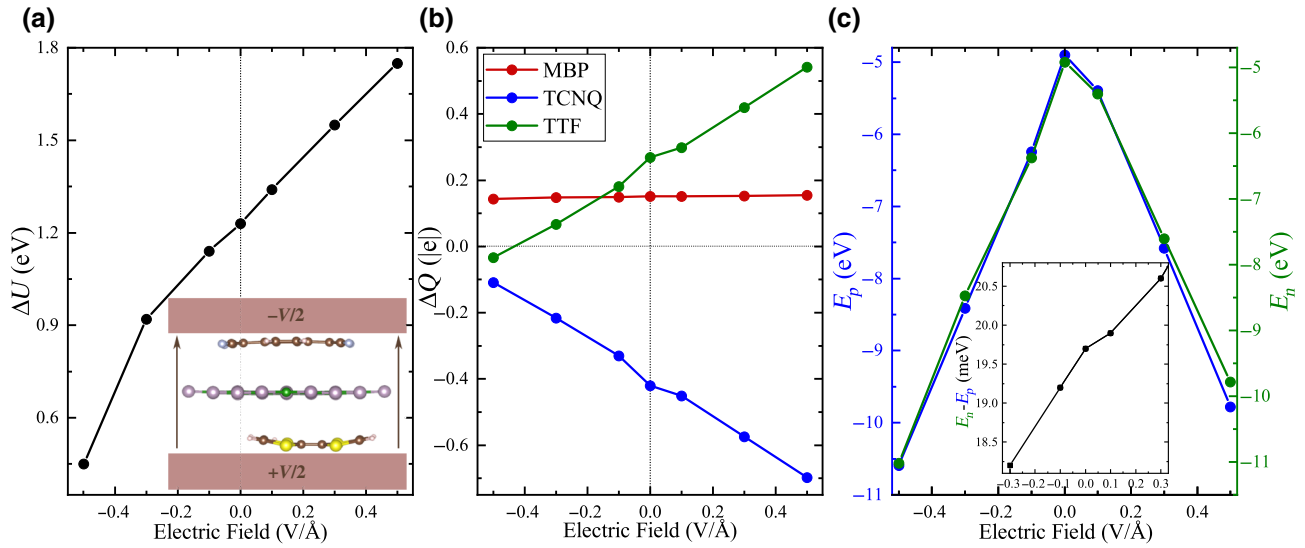
FIG. 5. (a) Potential difference ΔU (inset: the arrow represents the positive direction of the electric field in the structure), (b) Bader charge analysis, and (c) energy of localized states $E_{p,n}$ of TCNQ/MBP/TTF at different perpendicular electric field values with respect to vacuum energy.

clear from Fig. 3(b) that the charge distribution on MBP is lower, according to the molecules that lead to a *p-n* system, where MBP holds molecules without charge accumulation. On the other hand, charge redistribution is also low at interfacial regions of TCNQ/MBP and MBP/TTF; this can be linked with the low adsorption energy of molecules.

B. Electronic properties in the presence of electric field

The external electric field is an efficient method to tune the electronic properties of 2D structures [18–20,75–78]. In this section, an electric field that is perpendicular to TCNQ/MBP/TTF is considered to modulate the electronic properties of the *p-n* junction. A schematic representation of the electric field direction perpendicular to the plane of the TCNQ/MBP/TTF system is shown in the inset of Fig. 5(a). The direction of the arrow along the *z* axis shows the positive electric field from TTF to the TCNQ layer. The applied electric field changes the internal potential of the structure, charge distribution, and electronic bands, as depicted in Fig. 4 for the TCNQ/MBP/TTF junction.

Evaluation of the electronic bands in Figs. 4(a)–4(d) shows that a positive electric field does not change electronic bands significantly, while a negative field opens up an energy band gap of 0.42 eV between two localized states of TCNQ and TTF molecules at $E = 0.5$ V/Å. It is also clear that, while the *p* state is rather sensitive to negative electric fields, the shallow *n* state is almost unaffected. There is a physical limit to the magnitude of the external electric field due to the possibility of field emission of electrons into a vacuum [79]. The magnitudes of the vacuum and electric field are crucial parameters for

the applied electric field in DFT [49]. Here, we consider a fixed vacuum value for all structures. However, both the value and direction of the electric field are evaluated as variables to tune the electronic structure of the *p-n* system. The external electric field yields charge transfer and its increasing value gives rise to the enhancement of charge transfer between different layers. The increasing value of the electric field can yield electron field emission into the vacuum [79]. The charge density from the field emission mechanism at the edges of a vacuum can be followed from the differential charge density ($\Delta\rho_{\text{diff}}$; see Fig. S3 in the Supplemental Material [54] for differential charge density). It is clear from the value of $\Delta\rho_{\text{diff}}$ that the charge-transfer regime is more prominent from the negative electric field values and significant charge distribution is accumulated in the vacuum region for the electric field values of $E \geq 0.5$ V/Å and $E \leq -0.5$ V/Å, which determine the physical limits of electric field magnitude in this study (see the Supplemental Material [54] for the whole band spectrum of different electric field values). The energy band gap in Figs. 4(a) and 4(b) restricts electron conduction through the junction. On the other hand, due to the low energy band gap at positive electric field, electrons can flow at a low-bias voltage. This mechanism suggests the potential application of TCNQ/MBP/TTF as a rectifying *p-n* diode for low-dimensional circuits, which are analyzed in Sec. III C. The effect of the electric field on the electronic structure of TCNQ/MBP/TTF can also be followed from the charge-density difference in Figs. 4(e) and 4(f). Although a relatively weak perpendicular electric field $|E| < 0.3$ V/Å does not affect the band structure significantly, it changes the charge-density difference conspicuously. It is clear from Fig. 4 that charge redistribution and charge transfer

between molecules increases upon increasing the positive electric field, which supports the *p-n* character of this heterostructure. Accordingly, charge distribution decreases at negative electric field values and finally disappears at $E = 0.5$ V/Å. To present a qualitative discussion of the charge donation/acceptance of the molecules, Bader charges together with the $p(n)$ state energy and potential difference (ΔU) profile are analyzed in the presence of an electric field (Fig. 5).

Modulation of the band structure of the TCNQ/MBP/ TTF system under the perpendicular electric field can be understood by considering its local electrostatic potential profile, which shows the relative potential difference between molecules. It is revealed from Fig. 5(a) that the potential difference increases linearly with increasing values of electric field, but decreases with increasing negative electric field values in the range of -0.5 V/Å $\leq E \leq 0.5$ V/Å. Accordingly, the Bader charge analysis in Fig. 5(b) shows that the TCNQ molecule remains a charge-accepting molecule in positive and negative electric fields. On the other hand, for the donor TTF molecule, the net positive charge is reduced and becomes negative at $E = 0.5$ V/Å, where the structure no longer shows *p-n* characteristics. The *p-n* system is more sensitive to the magnitude of electric values in the negative direction (see Fig. S3 in the Supplemental Material [54] for differential charge density). Charge transfer (ΔQ) of TCNQ (TTF) increases (decreases) linearly with the electric field. It is also clear that the charge on MBP remains almost constant; this supports the idea of the *p-n* character, such that MBP does not accumulate charge and allows charge transfer between p (TCNQ) and n (TTF) states. Figure 5(c) shows the modulation of two localized states, E_p and E_n, from TCNQ and TTF molecules, respectively, relative to the vacuum energy level, as a function of electric field. The donor (acceptor)

state, E_n (E_p), decreases by applying an external electric field and the difference in localized states (band gap) is examined in the inset of Fig. 5(c) over the moderate electric field range. There is a tiny energy gap (approximately 20 meV) between E_p and E_n in the absence of the electric field, while $E_n - E_p$ increases upon increasing the external electric field.

C. Transport

The current-voltage characteristics of the proposed *p-n* junction are calculated by using a simplified TB model. In the TB model, we replace each adsorbed molecule and MBP with single electronic levels in a tight-binding scheme, as shown in the inset of Fig. 6(a). The flat electronic bands from TCNQ and TTF molecules in Fig. 2(d) confirm the single-level approximation. To calculate current-voltage characteristics, we attach two metallic electrodes on both sides of the TCNQ/MBP/TTF junction. The chemical potential of the whole *p-n* device, which depends on the electronic and chemical structure of the electrodes, is set in the middle of the TCNQ and TTF energy levels, as shown in the inset of Fig. 6(a). The on-site energies are set to $E_{p,n}$ for molecules and the edge of the conduction band for MBP from HSE06 calculations. The energy level of the MBP layer is far from the chemical potential level and does not contribute to the current at low voltages, as shown in the inset of Fig. 6(a). The applied electric field produces a potential difference between each layer, which is added as an additional on-site energy to each site. In the limit of isolated layers, there is no hopping between layers, and thus, there is no charge sharing. In the tight-binding approach, the interaction between layers can be modeled by using an additional hopping between layers, which enables charge transfer
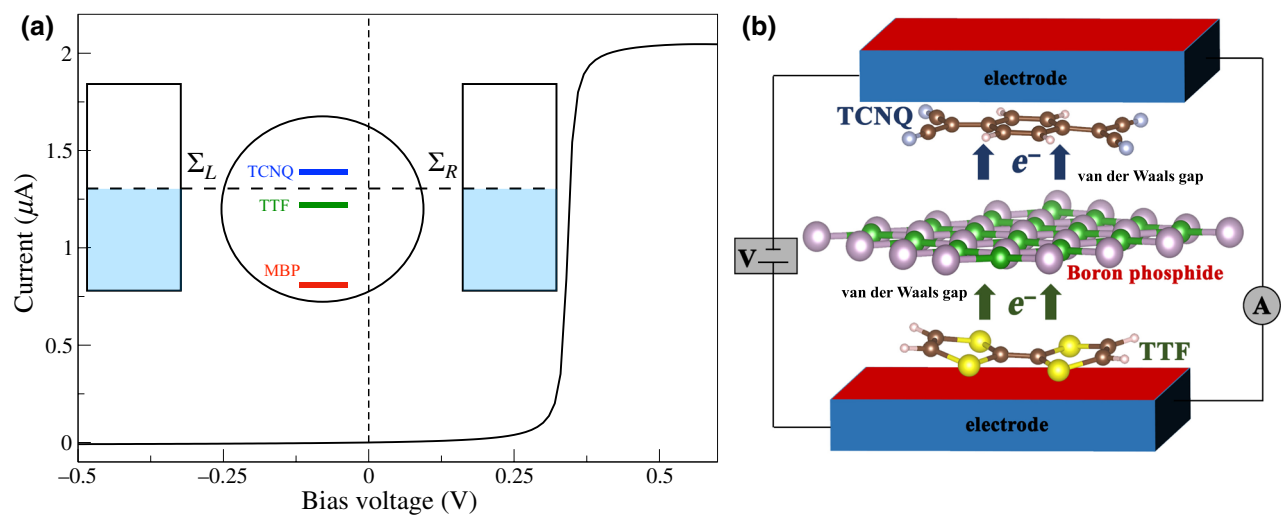

FIG. 6.   (a) The current-voltage characteristics of modeled TCNQ/MBP/TTF between two conducting electrodes. The inset presents the electronic levels of TCNQ, TTF, and MBP. (b) A schematic representation of the TCNQ/MBP/TTF *p-n* nanodiode.

between layers. Here, the value of hopping determines the amount of charge accumulation-depletion on layers. The obtained hopping value is 40 meV, which is close to that of interlayer hopping in bilayer graphene [80]. The imaginary part of self-energy reflects the coupling strength between TCNQ/MBP/TTF and electrodes. In the weak coupling regime, the value of $\Gamma_{L,R}$ should be much smaller than that of energy splitting between molecule levels. The $\Gamma_{L,R}$ value is set to 10 meV, which reflects possible weak van der Waals coupling between molecules and electrodes. Our results show the rectifying behavior in the current-voltage characteristics of the TCNQ/MBP/TTF TB model in Fig. 6(a). Due to different on-site energies, there is a potential barrier between two molecules. At negative bias, the applied voltage increases the potential barrier and prevents electron flow, while the barrier is removed at positive bias voltage and the current increases above a threshold voltage. The diode work voltage and breakdown voltage are around 0.5 V. For calculations with on-site energies from the GGA level, the breakdown voltage is reduced to nearly 50 mV; this is related to the small energy gap in the TCNQ/MBP/TTF junction (see the Supplemental Material [54] for current-voltage characteristics for GGA levels). According to the above results, we present a schematic of the proposed *p-n* nanoscale diode based on the adsorption of organic molecules on MBP in Fig. 6(b).

D. Optical properties

The optical properties of 2D nanostructures are important for future technological applications. The optical responses of TCNQ/MBP, MBP/TTF, and TCNQ/MBP/TTF are analyzed by calculating the imaginary part of the dielectric function [$\varepsilon_2(\omega)$], which is presented in Fig. 7. The absolute value of the imaginary part of the dielectric function for 2D monolayers depends on the arbitrary length of vacuum in the unit cell. Here, we normalize the dielectric function by multiplying it by vacuum length. Moreover, the optical response of MBP is also presented in Fig. 7 to specify the peaks arising from the MBP layer, as initially calculated in Refs. [15] and [16]. The absorption onsets of the adsorbed structures are all compatible with their small energy band gaps. It is clear from Fig. 7 that, although all three structures preserve the optical profile of MBP, molecular modifications yield some extra absorption peaks in the spectrum. MBP has two remarkable absorption peaks at around 2.5 eV and 6.5 eV and its absorption occurs in the visible and beyond UV ranges. Because of the adsorption of TCNQ, a new peak appears at around 0.36 eV, which indicates an optical absorption in the infrared (IR) region. This prominent effect of TCNQ is also discussed for adsorption on MoS_2 [31], arsenene [71], and phosphorene [30] 2D structures. On the other hand, the adsorption of TTF has negligible effects on the optical properties of the MBP/TTF system, as also shown
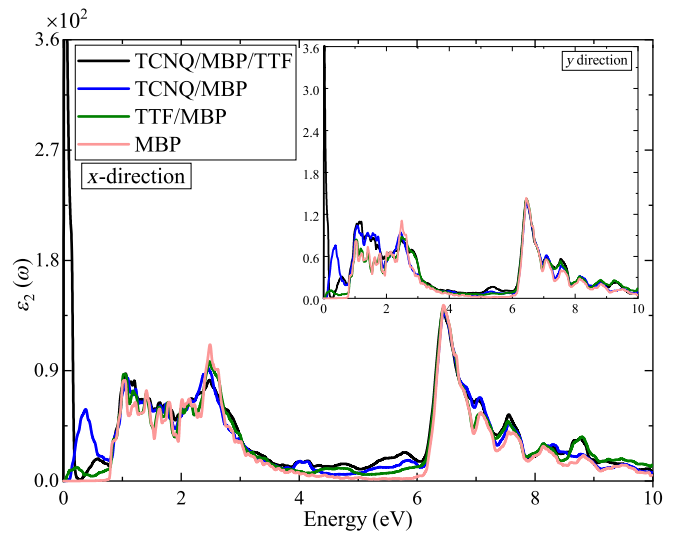

FIG. 7. Imaginary part of the dielectric function for MBP, TCNQ/MBP, MBP/TTF, and TCNQ/MBP/TTF structures. The values of the dielectric function are normalized to the vacuum length.

in Refs. [30] and [31]. Through the adsorption of two molecules, the optical spectrum of TCNQ/MBP/TTF gains a far-IR absorption peak, which is essential for the design of nanodevices based on IR technology. It can also be interpreted that the IR peak of TCNQ/MBP is redshifted and its absorption strength is enhanced by the adsorption of a TTF molecule, which results in a new optical character of the structure that is distinct from those of TCNQ/MBP and MBP/TTF. It is also known that DFT HSE yields a blueshift in the optical spectrum. The main absorption peak of TCNQ/MBP/TTF in the far-IR region is blueshifted by around 0.6 eV for HSE calculations (see the Supplemental Material [54] for details). The polarization axis of light is also important due to the anisotropy of the system. The imaginary part of the dielectric function along the *y* direction is plotted in the inset of Fig. 7. The optical properties of MBP are isotropic in the *xy* plane and the imaginary part of the dielectric is almost identical for the *x* and *y* directions. The molecular adsorption of TCNQ on MBP yields optical anisotropy in the *xy* plane and modifies the optical spectrum in the energy range between 0.0 and 2.5 eV for TCNQ/MBP and TCNQ/MBP/TTF. However, the TTF molecule does not have any substantial effects on the isotropy of the structure, as observed in the spectrum of MBP/TTF in Fig. 7. The anisotropy in the optical spectrum arising from TCNQ has also been reported previously in Ref. [30]. More sophisticated calculations can be performed by using models beyond DFT, such as GW and the Bethe-Salpeter equation (BSE), to observe the many-body effects in the optical spectrum. The local field effects are ignored due to their tremendous computational costs for such a large structure.

IV. CONCLUSION

In summary, by using density functional theory, we investigate the electronic characteristics of MBP through the physical adsorption of two different organic molecules. TCNQ and TTF molecules donate electrons and holes to the MBP layer and transform it into a p- and n-type semiconductor. We find the lowest energy atomic configuration for the adsorption of each molecule and calculate the electronic band structure, binding energy, potential barrier, and charge density in the new p and n semiconductor. We expand on the idea of molecular adsorption by simultaneous adsorption of both molecules on both sides of MBP (full coverage of MBP) toward a p-n junction with rectifying behavior. The transport properties of the p-n junctions are studied within a simple TB approach, by replacing each MBP layer and adsorbed molecule with a single TB site. The current-voltage characteristics obtained by using the Green function show an asymmetrical current and rectifying of the theoretically proposed p-n molecular device. Our study suggests a p-n mechanism for the full coverage of MBP with organic molecules; this tunes the electronic and optical properties of pristine MBP. As a result, upon molecular doping, the modification of MBP can be treated as a p-n junction, which builds up a featured component of semiconductor electronic devices. This results bring the possibility of the p-n junction design through full coverage of a 2D monolayer with molecules. In addition, the IR-sensitive nature of the TCNQ/MBP/TTF structure may result in it being a potential material for applications in optoelectronic devices.

[1] H. Liu, A. T. Neal, Z. Zhu, Z. Luo, X. Xu, D. Tománek, and P. D. Ye, Phosphorene: An unexplored 2D semiconductor with a high hole mobility, ACS Nano **8,** 4033 (2014).

[2] Z. Zhu and D. Tománek, Semiconducting Layered Blue Phosphorus: A Computational Study, Phys. Rev. Lett. **112,** 176802 (2014).

[3] Y. Mogulkoc, M. Modarresi, A. Mogulkoc, and Y. Ciftci, Electronic and optical properties of bilayer blue phosphorus, Comput. Mater. Sci. **124,** 23 (2016).

[4] A. Kara, H. Enriquez, A. P. Seitsonen, L. L. Y. Voon, S. Vizzini, B. Aufray, and H. Oughaddou, A review on silicene—new candidate for electronics, Surf. Sci. Rep. **67,** 1 (2012).

[5] M. Houssa, A. Dimoulas, and A. Molle, Silicene: A review of recent experimental and theoretical investigations, J. Phys.: Condens. Matter **27,** 253002 (2015).

[6] J. Deng, B. Xia, X. Ma, H. Chen, H. Shan, X. Zhai, B. Li, A. Zhao, Y. Xu, W. Duan, S.-C. Zhang, B. Wang, and J. G. Hou, Epitaxial growth of ultraflat stanene with topological band inversion, Nat. Mater. **17,** 1081 (2018).

[7] M. Liao, Y. Zang, Z. Guan, H. Li, Y. Gong, K. Zhu, X.-P. Hu, D. Zhang, Y. Xu, Y.-Y. Wang, K. He, X.-C. Ma, S.-C. Zhang, and Q.-K. Xue, Superconductivity in few-layer stanene, Nat. Phys. **14,** 344 (2018).

[8] M. Modarresi, A. Kakoee, Y. Mogulkoc, and M. Roknabadi, Effect of external strain on electronic structure of stanene, Comput. Mater. Sci. **101,** 164 (2015).

[9] J. Yuhara, B. He, N. Matsunami, M. Nakatake, and G. Le Lay, Graphene's latest cousin: Plumbene epitaxial growth on a "nano watercube", Adv. Mater. **31,** 1901017 (2019).

[10] S. Manzeli, D. Ovchinnikov, D. Pasquier, O. V. Yazyev, and A. Kis, 2D transition metal dichalcogenides, Nat. Rev. Mater. **2,** 17033 (2017).

[11] Z.-Y. Zhao and Q.-L. Liu, Study of the layer-dependent properties of MoS_2 nanosheets with different crystal structures by DFT calculations, Catal. Sci. Technol. **8,** 1867 (2018).

[12] K. Dileep, R. Sahu, S. Sarkar, S. C. Peter, and R. Datta, Layer specific optical band gap measurement at nanoscale in MoS_2 and ReS_2 van der waals compounds by high resolution electron energy loss spectroscopy, J. Appl. Phys. **119,** 114309 (2016).

[13] A. Sengupta, M. Audiffred, T. Heine, and T. A. Niehaus, Stacking dependence of carrier transport properties in multilayered black phosphorous, J. Phys.: Condens. Matter **28,** 075001 (2016).

[14] Y. Cai, G. Zhang, and Y.-W. Zhang, Layer-dependent band alignment and work function of few-layer phosphorene, Sci. Rep. **4,** 6677 (2014).

[15] Y. Mogulkoc, M. Modarresi, A. Mogulkoc, and B. Alkan, Electronic and optical properties of boron phosphide/blue phosphorus heterostructures, Phys. Chem. Chem. Phys. **20,** 12053 (2018).

[16] A. Mogulkoc, Y. Mogulkoc, M. Modarresi, and B. Alkan, Electronic structure and optical properties of novel monolayer gallium nitride and boron phosphide heterobilayers, Phys. Chem. Chem. Phys. **20,** 28124 (2018).

[17] M. Modarresi, A. Mogulkoc, Y. Mogulkoc, and A. Rudenko, Lateral Spin Valve Based on the Two-Dimensional CrN/P/CrN Heterostructure, Phys. Rev. Appl. **11,** 064015 (2019).

[18] W. Xiong, C. Xia, J. Du, T. Wang, Y. Peng, Z. Wei, and J. Li, Band engineering of the MoS_2/stanene heterostructure: Strain and electrostatic gating, Nanotechnology **28,** 195702 (2017).

[19] K. D. Pham, C. V. Nguyen, H. T. Phung, H. V. Phuc, B. Amin, and N. N. Hieu, Strain and electric field tunable electronic properties of type-ii band alignment in van der waals $GaSe$/$MoSe_2$ heterostructure, Chem. Phys. **521,** 92 (2019).

[20] J. Shi, Y. Ou, M. A. Migliorato, H. Wang, H. Li, Y. Zhang, Y. Gu, and M. Zou, Tuning the electronic structure of GeC/WS_2 van der waals heterostructure by electric field and strain: A first principles study, Comput. Mater. Sci. **160,** 301 (2019).

[21] S. Mouri, W. Zhang, D. Kozawa, Y. Miyauchi, G. Eda, and K. Matsuda, Thermal dissociation of inter-layer excitons in MoS_2/$MoSe_2$ hetero-bilayers, Nanoscale **9,** 6674 (2017).

[22] S. Pak, J. Lee, Y.-W. Lee, A.-R. Jang, S. Ahn, K. Y. Ma, Y. Cho, J. Hong, S. Lee, H. Y. Jeong, *et al.*, Strain-mediated interlayer coupling effects on the excitonic behaviors in an epitaxially grown MoS_2/WS_2 van der waals heterobilayer, Nano Lett. **17**, 5634 (2017).

[23] C. Zhang, C.-P. Chuu, X. Ren, M.-Y. Li, L.-J. Li, C. Jin, M.-Y. Chou, and C.-K. Shih, Interlayer couplings, moiré patterns, and 2D electronic superlattices in MoS_2/WSe_2 hetero-bilayers, Sci. Adv. **3**, e1601459 (2017).

[24] M. Sing, U. Schwingenschlögl, R. Claessen, P. Blaha, J. M. P. Carmelo, L. M. Martelo, P. D. Sacramento, M. Dressel, and C. S. Jacobsen, Electronic structure of the quasi-one-dimensional organic conductor TTF-TCNQ, Phys. Rev. B **68**, 125111 (2003).

[25] M. Yoon, Y. Miyamoto, and M. Scheffler, Enhanced dipole moments in photo-excited TTF–TCNQ dimers, New J. Phys. **13**, 073039 (2011).

[26] B. Mukherjee and M. Mukherjee, High performance organic thin film transistors with solution processed TTF-TCNQ charge transfer salt as electrodes, Langmuir **27**, 11246 (2011).

[27] R. Pauliukaite, A. Malinauskas, G. Zhylyak, and U. E. Spichiger-Keller, Conductive organic complex salt TTF-TCNQ as a mediator for biosensors. An overview, Electroanal.: Int. J. Devoted Fundam. Pract. Aspects Electroanal. **19**, 2491 (2007).

[28] Y. Lu, W. Chen, Y. Feng, and P. He, Tuning the electronic structure of graphene by an organic molecule, J. Phys. Chem. B **113**, 2 (2008).

[29] T. Hu and I. C. Gerber, Theoretical study of the interaction of electron donor and acceptor molecules with graphene, J. Phys. Chem. C **117**, 2411 (2013).

[30] Y. Jing, Q. Tang, P. He, Z. Zhou, and P. Shen, Small molecules make big differences: Molecular doping effects on electronic and optical properties of phosphorene, Nanotechnology **26**, 095201 (2015).

[31] Y. Jing, X. Tan, Z. Zhou, and P. Shen, Tuning electronic and optical properties of MoS_2 monolayer via molecular charge transfer, J. Mater. Chem. A **2**, 16892 (2014).

[32] D. Kiriya, M. Tosun, P. Zhao, J. S. Kang, and A. Javey, Air-stable surface charge transfer doping of MoS_2 by benzyl viologen, J. Am. Chem. Soc. **136**, 7853 (2014).

[33] M.-Y. Liu, Y. Huang, Q.-Y. Chen, C. Cao, and Y. He, Unexpected electronic structure of the alloyed and doped arsenene sheets: First-principles calculations, Sci. Rep. **6**, 29114 (2016).

[34] M. Pumera and Z. Sofer, 2D monoelemental arsenene, antimonene, and bismuthene: Beyond black phosphorus, Adv. Mater. **29**, 1605299 (2017).

[35] Q.-Q. Sun, Y.-J. Li, J.-L. He, W. Yang, P. Zhou, H.-L. Lu, S.-J. Ding, and D. Wei Zhang, The physics and backward diode behavior of heavily doped single layer MoS_2 based *pn* junctions, Appl. Phys. Lett. **102**, 093104 (2013).

[36] L. Huang, N. Huo, Y. Li, H. Chen, J. Yang, Z. Wei, J. Li, and S.-S. Li, Electric-field tunable band offsets in black phosphorus and MoS_2 van der waals pn heterostructure, J. Phys. Chem. Lett. **6**, 2483 (2015).

[37] Y. Deng, Z. Luo, N. J. Conrad, H. Liu, Y. Gong, S. Najmaei, P. M. Ajayan, J. Lou, X. Xu, and P. D. Ye, Black phosphorus–monolayer MoS_2 van der waals heterojunction *p–n* diode, ACS Nano **8**, 8292 (2014).

[38] L. Huang and J. Li, Tunable electronic structure of black phosphorus/blue phosphorus van der waals *pn* heterostructure, Appl. Phys. Lett. **108**, 083101 (2016).

[39] B. Cai, S. Zhang, Z. Yan, and H. Zeng, Noncovalent molecular doping of two-dimensional materials, ChemNanoMat **1**, 542 (2015).

[40] H. Liu, Y. Liu, and D. Zhu, Chemical doping of graphene, J. Mater. Chem. **21**, 3335 (2011).

[41] T. Lohmann, K. von Klitzing, and J. H. Smet, Four-terminal magneto-transport in graphene *pn* junctions created by spatially selective doping, Nano Lett. **9**, 1973 (2009).

[42] N. Gao, Y. Zhu, and Q. Jiang, Formation of arsenene *p–n* junctions via organic molecular adsorption, J. Mater. Chem. C **5**, 7283 (2017).

[43] D. Çakır, D. Kecik, H. Sahin, E. Durgun, and F. M. Peeters, Realization of a *p–n* junction in a single layer boron-phosphide, Phys. Chem. Chem. Phys. **17**, 13013 (2015).

[44] G. Kresse and J. Furthmüller, Efficiency of ab-initio total energy calculations for metals and semiconductors using a plane-wave basis set, Comp. Mat. Sci. **6**, 15 (1996).

[45] G. Kresse and J. Furthmüller, Efficient iterative schemes for *ab initio* total-energy calculations using a plane-wave basis set, Phys. Rev. B **54**, 11169 (1996).

[46] J. P. Perdew, K. Burke, and M. Ernzerhof, Generalized Gradient Approximation Made Simple, Phys. Rev. Lett. **77**, 3865 (1996).

[47] H. J. Monkhorst and J. D. Pack, Special points for Brillouin-zone integrations, Phys. Rev. B **13**, 5188 (1976).

[48] S. Grimme, Semi empirical GGA-type density functional constructed with a long-range dispersion correction, J. Comp. Chem. **27**, 1787 (2006).

[49] J. Neugebauer and M. Scheffler, Adsorbate-substrate and adsorbate-adsorbate interactions of Na and K adlayers on Al (111), Phys. Rev. B **46**, 16067 (1992).

[50] J. Heyd, G. E. Scuseria, and M. Ernzerhof, Hybrid functionals based on a screened coulomb potential, J. Chem. Phys. **118**, 8207 (2003).

[51] J. Heyd, G. E. Scuseria, and M. Ernzerhof, Erratum: "Hybrid functionals based on a screened coulomb potential" [J. Chem. Phys. **118**, 8207 (2003)], J. Chem. Phys. **124**, 219906 (2006).

[52] R. R. Pela, M. Marques, and L. K. Teles, Comparing LDA-1/2, HSE03, HSE06 and G0W0 approaches for band gap calculations of alloys, J. Phys.: Condens. Matter **27**, 505502 (2015).

[53] W. Chen and A. Pasquarello, Band-edge levels in semiconductors and insulators: Hybrid density functional theory versus many-body perturbation theory, Phys. Rev. B **86**, 035134 (2012).

[54] See the Supplemental Material at http://link.aps.org/supplemental/10.1103/PhysRevApplied.12.054036 for extended analysis by using DFT-HSE, charge partition (DDEC6 method) and perpendicular electric field. The adsorption energies of possible configurations are also presented.

[55] W. Tang, E. Sanville, and G. Henkelman, A grid-based bader analysis algorithm without lattice bias, J. Phys.: Condens. Matter **21**, 084204 (2009).

[56] E. Sanville, S. D. Kenny, R. Smith, and G. Henkelman, Improved grid-based algorithm for bader charge allocation, J. Comput. Chem. **28,** 899 (2007).

[57] G. Henkelman, A. Arnaldsson, and H. Jónsson, A fast and robust algorithm for bader decomposition of charge density, Comput. Mater. Sci. **36,** 354 (2006).

[58] M. Wimmer, Quantum transport in nanostructures: From computational concepts to spintronics in graphene and magnetic tunnel junctions (2009), PhD Thesis, University of Regensburg.

[59] S. Datta, *Quantum Transport: Atom to Transistor* (Cambridge University Press, New York, 2005).

[60] C. J. O. Verzijl, J. S. Seldenthuis, and J. M. Thijssen, Applicability of the wide-band limit in DFT-based molecular transport calculations, J. Chem. Phys. **138,** 094102 (2013).

[61] M. Gajdoš, K. Hummer, G. Kresse, J. Furthmüller, and F. Bechstedt, Linear optical properties in the projector-augmented wave methodology, Phys. Rev. B **73,** 045112 (2006).

[62] H. Şahin, S. Cahangirov, M. Topsakal, E. Bekaroglu, E. Akturk, R. T. Senger, and S. Ciraci, Monolayer honeycomb structures of group-IV elements and III–V binary compounds: First-principles calculations, Phys. Rev. B **80,** 155453 (2009).

[63] Q. Tang, Z. Zhou, and Z. Chen, Molecular charge transfer: A simple and effective route to engineer the band structures of BN nanosheets and nanoribbons, J. Phys. Chem. C **115,** 18531 (2011).

[64] M. Quintana, E. Vazquez, and M. Prato, Organic functionalization of graphene in dispersions, Acc. Chem. Res. **46,** 138 (2012).

[65] S. Presolski and M. Pumera, Covalent functionalization of MoS_2, Mater. Today **19,** 140 (2016).

[66] K. Liu, L. Liu, Y. Luo, and D. Jia, One-step synthesis of metal nanoparticle decorated graphene by liquid phase exfoliation, J. Mater. Chem. **22,** 20342 (2012).

[67] L. Zhang, L.-F. Gao, L. Li, C.-X. Hu, Q.-Q. Yang, Z.-Y. Zhu, R. Peng, Q. Wang, Y. Peng, J. Jin, *et al.*, Negatively charged 2D black phosphorus for highly efficient covalent functionalization, Mater. Chem. Front. **2,** 1700 (2018).

[68] N. G. Limas and T. A. Manz, Introducing DDEC6 atomic population analysis: Part 2. Computed results for a wide range of periodic and nonperiodic materials, RSC Adv. **6,** 45727 (2016).

[69] T. A. Manz, Introducing DDEC6 atomic population analysis: Part 3. Comprehensive method to compute bond orders, RSC Adv. **7,** 45552 (2017).

[70] Y. Shi, K. K. Kim, A. Reina, M. Hofmann, L.-J. Li, and J. Kong, Work function engineering of graphene electrode via chemical doping, ACS Nano **4,** 2689 (2010).

[71] M. Sun, J.-P. Chou, J. Gao, Y. Cheng, A. Hu, W. Tang, and G. Zhang, Exceptional optical absorption of buckled arsenene covering a broad spectral range by molecular doping, ACS Omega **3,** 8514 (2018).

[72] N. Gao, G. Y. Lu, Z. Wen, and Q. Jiang, Electronic structure of silicene: Effects of the organic molecular adsorption and substrate, J. Mater. Chem. C **5,** 627 (2017).

[73] T.-C. Tseng, C. Urban, Y. Wang, R. Otero, S. L. Tait, M. Alcamí, D. Écija, M. Trelka, J. M. Gallego, N. Lin, *et al.*, Charge-transfer-induced structural rearrangements at both sides of organic/metal interfaces, Nat. Chem. **2,** 374 (2010).

[74] M. M. Menamparambath, J.-H. Park, H.-S. Yoo, S. P. Patole, J.-B. Yoo, S. W. Kim, and S. Baik, Large work function difference driven electron transfer from electrides to single-walled carbon nanotubes, Nanoscale **6,** 8844 (2014).

[75] S. Jiang, J. Shan, and K. F. Mak, Electric-field switching of two-dimensional van der waals magnets, Nat. Mater. **17,** 406 (2018).

[76] X.-P. Wang, X.-B. Li, N.-K. Chen, J.-H. Zhao, Q.-D. Chen, and H.-B. Sun, Electric field analyses on monolayer semiconductors: The example of InSe, Phys. Chem. Chem. Phys. **20,** 6945 (2018).

[77] G. Liu, G. Zhou, and Y.-H. Chen, Modulation of external electric field on surface states of topological insulator Bi_2Se_3 thin films, Appl. Phys. Lett. **101,** 223109 (2012).

[78] M. Ezawa, A topological insulator and helical zero mode in silicene under an inhomogeneous electric field, New J. Phys. **14,** 033003 (2012).

[79] P. J. Feibelman, Surface-diffusion mechanism versus electric field: Pt/Pt(001), Phys. Rev. B **64,** 125403 (2001).

[80] J. Jung and A. H. MacDonald, Accurate tight-binding models for the π bands of bilayer graphene, Phys. Rev. B **89,** 035405 (2014).